THE JOURNAL OF PHYSICAL CHEMISTRY B

Article

Cite This: J. Phys. Chem. B 2018, 122, 12219−12226

pubs.acs.org/JPCB

Structure and Chemical Order in S−Se Binary Glasses

Bing Yuan,[†] Weidi Zhu,[†] Ivan Hung,[‡] Zhehong Gan,[‡] Bruce Aitken,[§] and Sabyasachi Sen*[,†]

[†]Department of Materials Science & Engineering, University of California at Davis, Davis, California 95616, United States

[‡]Center of Interdisciplinary Magnetic Resonance, National High Magnetic Field Laboratory, 1800 East Paul Dirac Drive, Tallahassee, Florida 32310, United States

[§]Science & Technology Division, Corning Inc., Corning, New York 14831, United States

ABSTRACT: The compositional evolution of the structure and chemical order in binary S_xSe_{100-x} glasses ($0 \le x \le 90$) is investigated using a combination of high-resolution 2D ^{77}Se isotropic−anisotropic correlation NMR and Raman spectroscopy. The results indicate that the structure of S−Se glasses consists of two types of topological elements, namely polymeric $[Se,S]_n$ chains and eight-membered Se_yS_{8-y} rings ($0 \le y \le 8$). The relative concentration of Se atoms monotonically decreases in the chain elements and concomitantly increases in the ring elements with increasing S concentration. Moreover, the Se speciation results are consistent with an average heterocyclic ring composition of Se_1S_7 at low S content (≤40 at. % S), while the composition shifts to $Se_{1.5}S_{6.5}$ at higher S content (≥60 at. % S), indicating increasing incorporation of multiple Se atoms in each ring element. The Raman spectra suggest that −Se−Se− association is favored, when more than one Se atom is incorporated in chains and rings. As in their elemental forms, the S and Se atoms retain their preference of forming rings and chains in binary S_xSe_{100-x} glasses, which predicts a linear compositional variation in the relative fractions of these topological elements. This structural evolution is consistent with the corresponding variation in the T_g and molar volume, both of which exhibit a linear decrease with increasing S concentration.

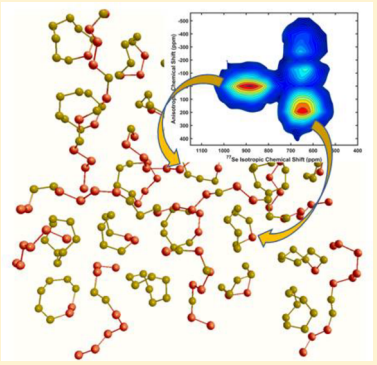

1. INTRODUCTION

Chalcogenide glasses consist of one or more of the chalcogen elements S, Se, and Te and constitute an important class of optical materials that has received great attention for a wide range of applications in photonics, nonvolatile memories, and remote sensing.[1−3] The elemental chalcogens, i.e., S, Se, and Te, are also glass-formers by themselves, and their structure−property relations have been extensively investigated. The most stable form of S is its orthorhombic polymorph (α-S) which transforms to the monoclinic form (β-S) at 95.6 °C, and the latter undergoes melting at 119 °C.[4] The structural building blocks in both α-S and β-S polymorphs are eight-membered S_8 rings. The structure of glassy S obtained from quenching the melt also consists predominantly of these S_8 ring molecules. Molten sulfur is characterized by a rather unique property known as living polymerization, which corresponds to a reversible transformation between S_8 ring molecules and $[S]_n$ chains at 159 °C.[5,6] The transformation of S_8 rings to $[S]_n$ chains results in a relatively sudden rise in viscosity with increasing temperature beyond the transition point.[7] Consequently, this transition renders the chain:ring ratio in glassy sulfur dependent on the cooling rate of the melt.[8] Se is chemically similar to S as the former can also exist in crystalline structures which are made of Se_8 rings, namely, the monoclinic polymorphs α-Se and β-Se. However, the most stable and commonly occurring polymorph of Se has a trigonal crystal structure consisting of covalently bonded parallel helical $[Se]_n$ chains.[9] Although the structure of glassy Se remained controversial in the past regarding its ring vs chain content, recent two-dimensional (2D) ^{77}Se nuclear magnetic resonance (NMR) spectroscopic studies have conclusively demonstrated that the structure of glassy Se essentially consists solely of $[Se]_n$ chains.[10] The element Te crystallizes in a hexagonal structure with spiral $[Te]_n$ chain elements, which is analogous to trigonal Se. However, compared to Se, the shorter second neighbor interaction distance in crystalline Te leads to quasi-metallic behavior.[4,11] This enhanced metallic character results in an extremely poor glass-forming ability for Te compared to that for S and Se. Similar to glassy selenium, the structure of amorphous Te is also composed of disordered $[Te]_n$ chains, but with significantly weaker interchain interaction.[12]

Structural studies have also been extended in the past to binary chalcogen systems. In particular, several excellent studies were reported on the structure of binary Se−Te glasses. It may be noted here that Se and Te can form a continuous solid solution where Se and Te atoms are believed to form composite chains in the crystal structure.[13] In a more recent study of Se−Te glasses, Bureau et al. used ^{77}Se NMR to demonstrate a random distribution of Se and Te atoms in the chain elements, with some preference for heteropolar bonding.[14] Tverjanovich et al. used a combination of Raman spectroscopy and density functional theory based calculations of the vibrational spectra to confirm this structural model of Se−Te glasses.[15]

Received: October 15, 2018
Revised: November 24, 2018
Published: November 28, 2018

DOI: 10.1021/acs.jpcb.8b10052
J. Phys. Chem. B 2018, 122, 12219−12226

Unlike the Se−Te system, where the size and the bonding preferences of the two elements are similar, S and Te constitute a binary system where the elements are quite different in size and electronegativity. Whereas Te prefers to form $[Te]_n$ chains, S prefers to form S_8 rings. As a consequence of these differences between S and Te and of the metallic nature of Te itself, the formation of homogeneous binary S−Te glasses is rather challenging, although a previous study claimed to have been able to obtain glasses over a limited composition range (20−50% Te) by splat quenching.[16]

The structural evolution in the S−Se binary system, on the other hand, has been studied primarily in the crystalline and molten states and on quenched products dissolved in CS_2, using X-ray diffraction, Raman, and ^{77}Se NMR spectroscopy.[17−20] Unfortunately, the structural disorder in the S_xSe_{100-x} crystals did not allow for the determination of atom positions via diffraction measurements.[21] The spectroscopic studies of crystalline and molten S_xSe_{100-x} indicated the presence of a mixture of Se_yS_{8-y} ring molecules, with S_7Se being the predominant molecular species at low Se concentration (≤25 at. % Se), while the concentration of S_6Se_2 molecules became comparable to the latter at ∼40 at. % Se.[19,20] Moreover, it was suggested that the Se atoms prefer to form Se−Se linkages in the S_6Se_2 molecules.[19,21] Additionally, ^{77}Se NMR of molten S_xSe_{100-x} indicated that a significant fraction of Se and S atoms take part in polymeric structural moieties in the form of $[Se,S]_n$ chains. However, to the best of our knowledge, no systematic structural study of glasses in this system has been reported in the literature to date.

In this study, we report the results of a structural investigation of binary S_xSe_{100-x} glasses with $0 \leq x \leq 90$, using Raman spectroscopy and high-resolution 2D magic-angle-turning phase adjusted spinning sideband (MATPASS) ^{77}Se NMR spectroscopy.[22] The 2D ^{77}Se MATPASS NMR spectra allow for the identification and quantitation of different Se environments in glasses with high accuracy based on the separation of isotropic and anisotropic chemical shift in two different dimensions and the correlation between them. The compositional evolution of the chain and molecular topological elements thus obtained is used to build a structural model of these glasses that is shown to be consistent with their thermophysical properties, namely, molar volume and glass transition temperature T_g.

2. EXPERIMENTAL SECTION

2.1. Sample Preparation. Binary S_xSe_{100-x} glasses with x = 0, 10, 30, 45, 60, 75, and 90 were synthesized in 7−15 g batches using the conventional melt quench method. Elemental sulfur and selenium (Alfa Aesar, 99.999%) were mixed together in stoichiometric ratios and subsequently flame-sealed in evacuated (10^{-4} Torr) quartz ampules. The fused ampules were placed in a rocking furnace, slowly heated to 673 K over 8 h, and subsequently held at this temperature and rocked for 48 h. The melts were then quenched by dipping the ampules in water.

2.2. 2D ^{77}Se MATPASS/CPMG NMR Spectroscopy. The 2D ^{77}Se MATPASS NMR spectra for all glasses were acquired at the National High Magnetic Field Laboratory using a 63 mm bore 18.8 T magnet equipped with a Bruker Avance III HD console operating at the resonance frequency of 152.7 MHz for ^{77}Se. Glass samples were crushed and packed into 3.2 mm ZrO_2 rotors and were spun at 10 kHz. Samples with high S content (S ≥ 45 at. %) are soft and malleable at ambient temperature and therefore were blended with small pieces of dry ice to crush into powder. All ^{77}Se NMR data were collected at 263 K to avoid heating of these glass samples above their T_g during magic-angle spinning (MAS). The pulse sequence used a series of five MAT π-pulses (4.0 μs) with incremented interpulse delays according to the timings detailed by Hung et al.[22] The method of States et al.[23] for hypercomplex data acquisition was applied to the Carr−Purcell−Meiboom−Gill (CPMG) pulse phase and the receiver phase. Acquisition consisted of 16 hypercomplex t_1 increments each with 24 transients and 90 s recycle delay. A total of 30 CPMG echoes were coadded for signal:noise improvement before the processing of 2D spectra. All spectra were externally referenced by recording the ^{17}O signal of natural abundance H_2O and then using the appropriate frequency ratio reported in the IUPAC recommendations.[24]

The ^{77}Se chemical shift anisotropy (CSA) tensors reported here follow the Haeberlen convention[25] defined as

$$|\delta_{zz} - \delta_{iso}| \geq |\delta_{xx} - \delta_{iso}| \geq |\delta_{yy} - \delta_{iso}|$$

$$\delta_{iso} = \frac{1}{3}(\delta_{zz} + \delta_{xx} + \delta_{yy})$$

$$\Delta = \delta_{zz} - \delta_{iso}$$

$$\eta = \frac{\delta_{yy} - \delta_{xx}}{\Delta}$$

where δ_{xx}, δ_{yy}, and δ_{zz} are the principal components of the chemical shift tensor and δ_{iso} is the isotropic chemical shift. The magnitude of the CSA is Δ, and its asymmetry is denoted as η.

2.3. Density and T_g Measurement. The density of S_xSe_{100-x} glasses was measured using a Micromeritics Accupyc II gas expansion pycnometer under a helium environment of 6N purity. Each measurement was performed on ∼2.0 g of sample loaded into a 1 cm^3 cup. Density values reported in this study are averages of 10 consecutive measurements at room temperature. The glass transition temperature T_g of the S_xSe_{100-x} glasses was measured using a Mettler-Toledo DSC1 differential scanning calorimeter. Approximately 15 mg of glass was loaded in a hermetically sealed 40 μL aluminum crucible, and scans were performed at 10 °C/min under a flowing nitrogen environment. T_g was determined to within ±2 °C as the onset of the glass transition.

2.4. Raman Spectroscopy. The Raman spectra of all glasses were collected in backscattering geometry with a resolution of 1 cm^{-1} using a Renishaw 1000 Raman microscope system equipped with a diode laser operating at a wavelength of 785 nm. Backscattered light was detected using a charge-coupled device cooled at 200 K.

3. RESULTS AND DISCUSSION

3.1. Physical Properties. The T_g, density, and molar volume of all S_xSe_{100-x} glasses are listed in Table 1, and the compositional variation is displayed in Figure 1. These results are in good agreement with the previously reported values in the literature.[26−29] Both T_g and molar volume of these glasses decrease approximately linearly with increasing S content (Figure 1). This trend in molar volume for S_xSe_{100-x} glasses is reflected in a similar trend in the crystalline state, as exemplified by orthorhombic sulfur and trigonal selenium

DOI: 10.1021/acs.jpcb.8b10052
J. Phys. Chem. B 2018, 122, 12219−12226

Table 1. Glass Transition Temperature T_g, Density, and Molar Volume of S_xSe_{100-x} Glasses

composition	T_g (±2.0 °C)	density (±0.002 g/cm^3)	molar volume (cm^3/mol)
Se	38.8	4.270	18.49 ± 0.01
$S_{10}Se_{90}$	30.5	4.063	18.28 ± 0.01
$S_{30}Se_{70}$	20.7	3.612	17.97 ± 0.01
$S_{45}Se_{55}$	14.4	3.275	17.67 ± 0.01
$S_{60}Se_{40}$	4.0	2.916	17.43 ± 0.02
$S_{75}Se_{25}$	−7.1	2.548	17.19 ± 0.03
$S_{90}Se_{10}$	−18.5		

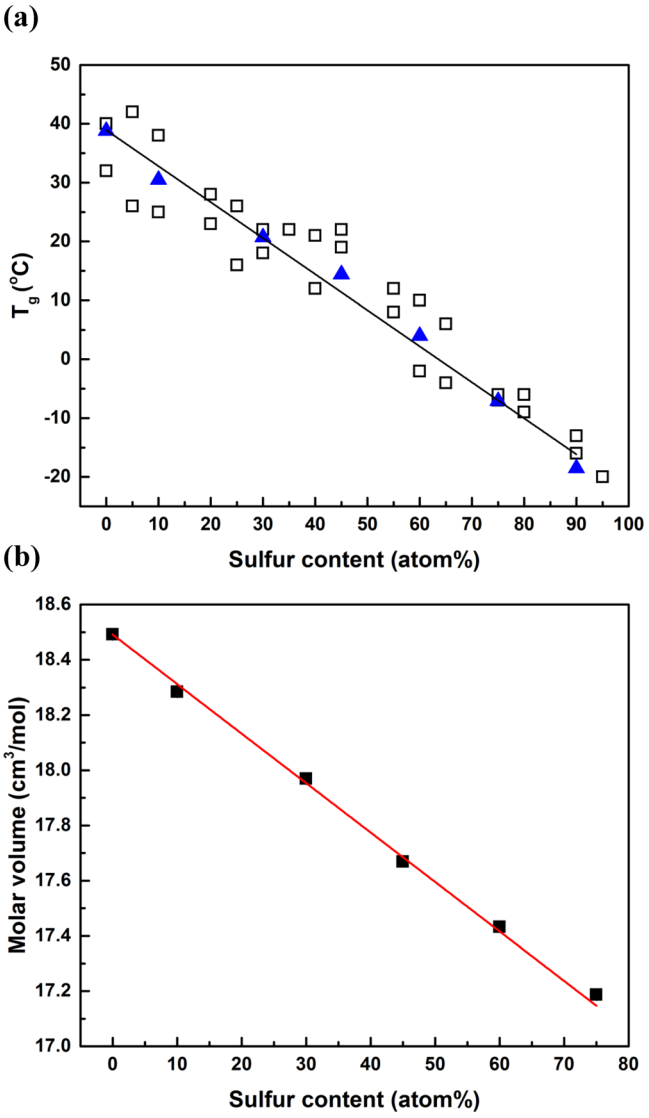

Figure 1. (a) T_g values of binary S_xSe_{100-x} glasses obtained in this study (filled triangles) and values reported in the literature[26−29] (open squares). (b) Molar volume of binary S_xSe_{100-x} glasses determined in this study. Straight lines through the data points in (a) and (b) represent linear least-squares fits to the data collected in this study.

with molar volumes of 15.50 and 16.45 cm^3/mol, respectively.[30,31] It is now well established in the literature that while the structure of amorphous S is predominantly composed of S_8 molecular rings, that of amorphous Se consists practically exclusively of polymeric $[Se]_n$ chains, with chain lengths on the order of ∼200 atoms.[8,10,32] Therefore, if S and Se maintain their preference in binary S_xSe_{100-x} glasses to form respectively rings and chains, then progressive addition of S to Se should result in a concomitant replacement of polymeric chains with ring molecules. Such compositional variation of the atomic structure is expected to result in a progressive weakening of the chain−chain interaction as they get interspersed with weakly bonded molecules and, thus, is consistent with the observed linear decrease in T_g and in the atomic packing efficiency of S_xSe_{100-x} glasses with increasing S content (Figure 1).

3.2. ^{77}Se NMR. Typical examples of ^{77}Se 2D MATPASS/CPMG NMR spectra of S_xSe_{100-x} glasses are shown in Figure 2. The 2D MATPASS experiment separates spinning sidebands along the anisotropic dimension and projects the isotropic spectra to the other dimension as if the spinning speed is infinitely fast (Figure 2a). The ^{77}Se isotropic NMR spectrum of glassy Se displays a single broad resonance centered at ∼850 ppm that corresponds to the −Se−**Se**−Se− environment in $[Se]_n$ chains, consistent with previous literature reports (Figure 2b).[10,33] Addition of S to Se results in the shift of the peak position of this resonance to ∼880−900 ppm and in the appearance of a second well-resolved resonance in the isotropic ^{77}Se NMR spectra that is centered at δ_{iso} ∼ 640−660 ppm (Figure 2b). This second resonance increases monotonically in relative intensity with progressive increase in S content (Figure 2b). The shift of the amorphous Se resonance to higher ppm (higher frequency) values upon addition of sulfur is indicative of the effect of incorporation of S atoms into the $[Se]_n$ chains. It was shown in a previous ^{77}Se NMR study of S_xSe_{100-x} melts by Chivers et al. that progressive replacement of Se nearest neighbors by S in $[Se]_n$ chains, i.e., the formation of −Se−**Se**−S− and −S−**Se**−S− linkages, results in the shift of the corresponding ^{77}Se resonance to higher frequencies.[20] Moreover, Chivers et al. also demonstrated that the ^{77}Se δ_{iso} for the Se sites in Se_yS_{8-y} ring molecules ranges between 600 and 730 ppm in S_xSe_{100-x} melts. This assignment is consistent with the range of 530−670 ppm recently reported for −Se−**Se**−Se− sites in Se_8 rings in the crystalline monoclinic allotrope α-Se.[10]

Further insight into the structural assignment of these ^{77}Se resonances in the isotropic NMR spectra of S_xSe_{100-x} glasses can be gained by considering the corresponding chemical shift tensor parameters Δ and η, which can be obtained from simulation of the corresponding spinning sideband spikelet pattern in the anisotropic dimension (Figure 3).[34] The simulation of the anisotropic slices at and around δ_{iso} ∼ 850 ppm results in average values of Δ ≈ −153 ppm and η ≈ 0.80. These Δ and η values are completely consistent with those reported for the −Se−**Se**−Se− environment in $[Se]_n$ chains in amorphous Se.[35] On the other hand, the simulation of slices at and around δ_{iso} ∼ 650 ppm yields a rather different average Δ and η of ≈−500 ppm and ≈0.15, respectively (Figure 4). These Δ and η values are quite comparable with those (Δ ranging between −430 and −450 ppm and η ranging between 0.2 and 0.4) recently reported for −Se−**Se**−Se− sites in Se_8 rings in α-Se.[10] Taken together, the δ_{iso}, Δ, and η values for the two ^{77}Se resonances in the isotropic NMR spectra of S_xSe_{100-x} glasses in Figure 2b suggest that the replacement of nearest-neighbor Se with S in Se_yS_{8-y} rings and $[Se]_n$ chains has a relatively minor effect on the anisotropy parameters Δ and η. To test this hypothesis, we have performed *ab initio* calculations of the ^{77}Se chemical shift tensor parameters for such Se environments in Se_yS_{8-y} ring molecules using the gauge-including projector augmented wave (GIPAW) method.[36] The −S−**Se**−S− environments were obtained by

DOI: 10.1021/acs.jpcb.8b10052
J. Phys. Chem. B 2018, 122, 12219−12226

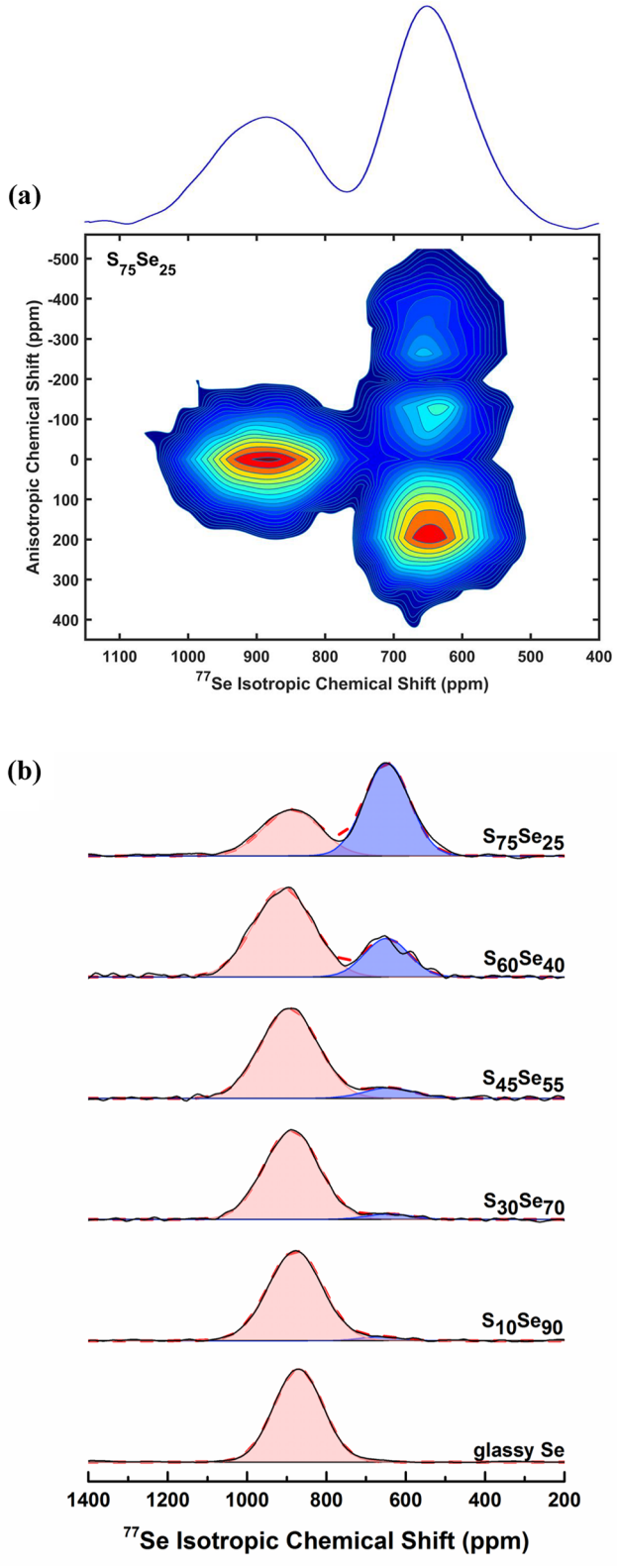

Figure 2. ^{77}Se NMR spectra of S_xSe_{100-x} glasses. (a) Representative 2D ^{77}Se MATPASS/CPMG NMR spectrum of $S_{75}Se_{25}$ glass with total projection along isotropic dimension (solid blue line). (b) Experimental (solid black line) and simulated (red dashed line) ^{77}Se isotropic NMR spectra of S_xSe_{100-x} glasses with compositions denoted alongside the spectra. Gaussian simulation components are shown in pink and blue.

replacing the S2 site with Se, and the −Se−**Se**−S− environments were obtained by simultaneously replacing the S2 and the S3 sites with Se in the S_8 molecules in crystalline orthorhombic sulfur.[37] These structures were then optimized, by allowing the atomic coordinates to vary, using density functional theory as implemented in the code CASTEP (Biovia Inc.) within the generalized gradient approximation (GGA) and with the PBE (Perdew−Burke−Ernzerhof) exchange-correlation functional.[38,39] Forces less than ∼30 meV Å^{-1} were observed at the end of the optimization process. The ^{77}Se chemical shift calculations were performed on these optimized structures using the code CASTEP-NMR within the GGA and with an energy cutoff of 600 eV.[36] Ultrasoft pseudopotentials were used to describe core−valence interactions. The Brillouin zone was sampled using the Monkhorst−Pack scheme and a 4 × 4 × 4 k-point grid. The isotropic chemical shift δ_{iso} was obtained from isotropic shielding σ_{iso} using the relationship $\delta_{iso} = -(\sigma_{iso} - \sigma_{ref})$, where σ_{ref} is the isotropic shielding of a reference material. The trigonal allotrope of Se was used as a reference, and the calculated ^{77}Se σ_{iso} of 784 ppm is equated to the experimental δ_{iso} value of 795 ppm for the single Se site in this allotrope. We have shown in previous studies that such calculations yield fairly accurate estimates of the ^{77}Se δ_{iso} and Δ in the chain (trigonal) and ring (monoclinic) allotropes of Se, except the calculated value of Δ needs to be scaled down by a factor of 2.[10] The present calculations yield comparable values of ^{77}Se δ_{iso} (550−570 ppm), Δ (−430 ppm), and η (0.15−0.30) for the −Se−**Se**−S− and −S−**Se**−S− environments in Se_yS_{8-y} rings, and these parameters are also similar to those characteristic of the −Se−**Se**−Se− environments in Se_8 rings in α-Se, as noted above. Therefore, the ^{77}Se resonance at $\delta_{iso} \sim$ 640−660 ppm may correspond to any one or all of these ring environments.

Additional constraints on the average stoichiometry of the Se_yS_{8-y} rings in these glasses can be imposed from the simulation of these ^{77}Se isotropic NMR spectral line shapes in Figure 2b with two components to yield the relative fractions of the Se atoms in chain and in ring environments from the peak integrals. The compositional evolution of the ratio of these two Se environments is shown in Figure 5, which indicates that for compositions near pure Se, most of the Se atoms reside in a chain environment. On the other hand, for glasses with composition near pure S, the majority of the Se atoms are found in a ring environment, attesting to the strong preference of S atoms to form S_8 rings. It is therefore reasonable to propose a structural model where in a glass of composition S_xSe_{100-x} there are $x/8$ eight-membered rings per formula unit, and on an average each such ring can accommodate y Se atoms, i.e., these are Se_yS_{8-y} rings. This model is equivalent to the substitution of y S atoms in each of the $x/8$ S_8 rings with y Se atoms. The substituted S atoms are incorporated into $[Se,S]_n$ chains. In this scenario, in one formula unit of the S_xSe_{100-x} glass there are $(x{\cdot}y/8)$ Se atoms in rings and $[(100 - x) - (x{\cdot}y/8)]$ Se atoms in chains. The ring versus chain Se speciation predictions of this structural model for $y = 1$ and $y = 1.5$ are compared with the experimentally observed Se speciation data in Figure 5. It is clear from Figure 5 that the model prediction for $y = 1$ agrees rather well with the experimental Se speciation for S concentrations of up to 40 at. %. However, at higher S concentrations of ≥60 at. %, the experimental speciation is closer to the model prediction for $y = 1.5$. Therefore, the chain versus ring speciation data for Se, as obtained from ^{77}Se NMR,

DOI: 10.1021/acs.jpcb.8b10052
J. Phys. Chem. B 2018, 122, 12219−12226

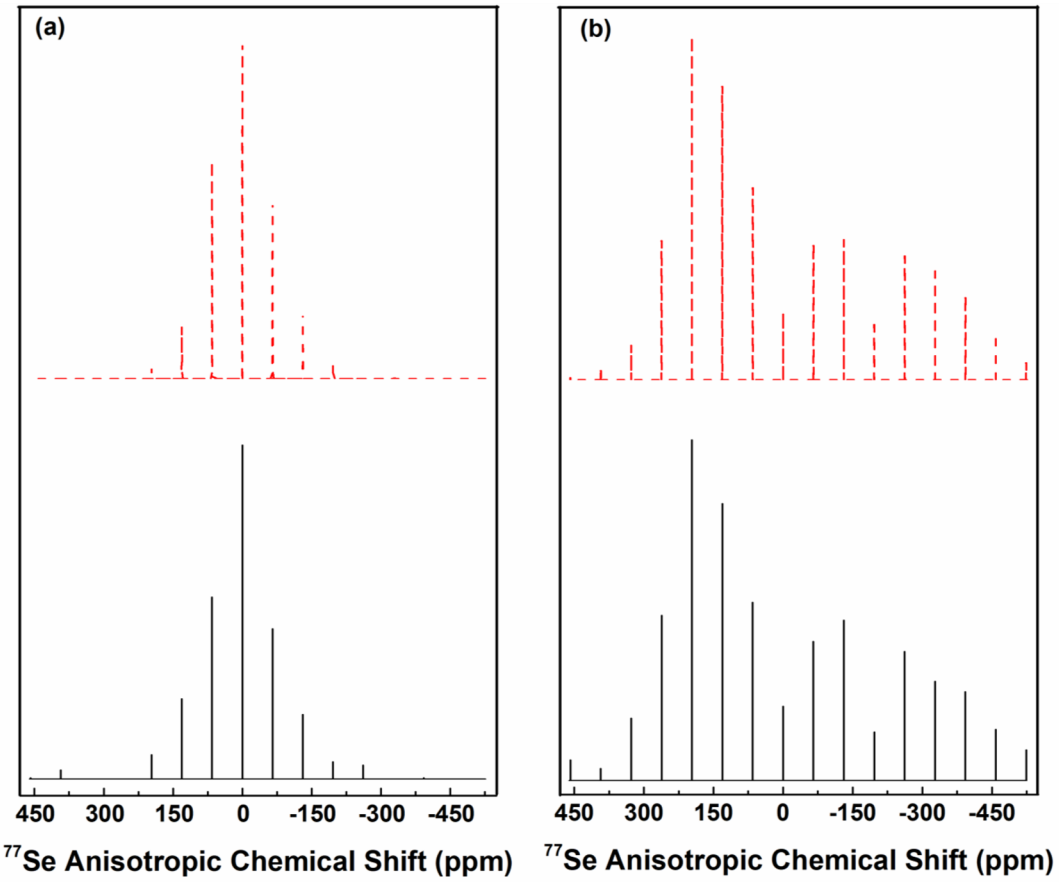

Figure 3. Comparison of experimental (bottom) and simulated (top) anisotropic ^{77}Se NMR spinning sideband intensities of $S_{75}Se_{25}$ glass taken at (a) δ_{iso} = 887 ppm and (b) δ_{iso} = 651 ppm.

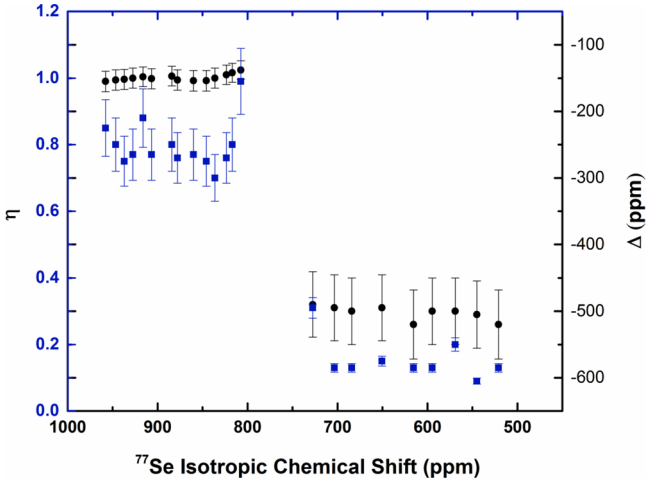

Figure 4. Representative ^{77}Se chemical shift tensor parameters Δ (circles) and η (squares) as a function of isotropic chemical shift, shown here for $S_{75}Se_{25}$ glass.

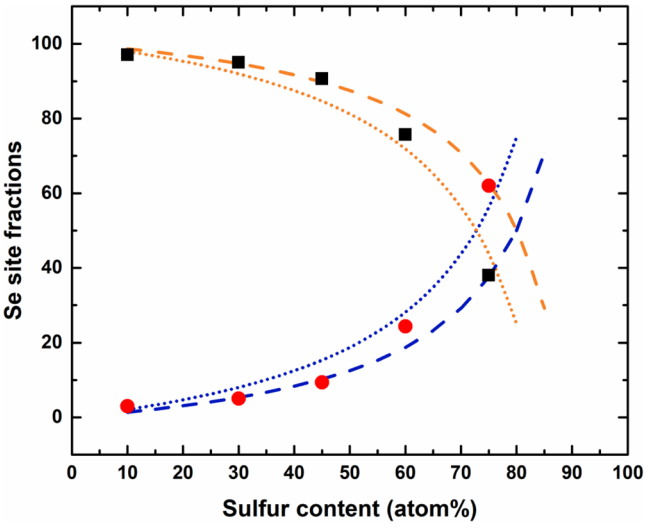

Figure 5. Compositional variation of Se site fractions in chains (squares) and rings (circles) obtained from simulations of ^{77}Se isotropic NMR spectra. Dashed (dotted) orange and blue lines are Se site fractions in chains and rings, respectively, expected from the structural model proposed in this study, for an average ring composition of Se_1S_7 ($Se_{1.5}S_{6.5}$). See the text for details.

are consistent with an average heterocyclic ring composition of Se_1S_7 for glasses with up to 40 at. % S. Further addition of S promotes increasing incorporation of Se atoms in Se_yS_{8-y} rings, such that the average ring composition becomes $Se_{1.5}S_{6.5}$ for glasses with ≥60 at. % S. It is to be noted that an average ring composition of Se_1S_7 does not preclude the presence of Se_2S_6 rings since some of these eight-membered rings may be homocyclic, i.e., S_8 rings, and a coexistence of S_8, Se_1S_7, and Se_2S_6 rings may be entropically favored in a glass. However, the Se ring speciation in glasses, as obtained in this study from ^{77}Se NMR, shows a trend that is opposite of that previously reported in S_xSe_{100-x} melts by Chivers et al.[20] Those authors

DOI: 10.1021/acs.jpcb.8b10052
J. Phys. Chem. B 2018, 122, 12219−12226

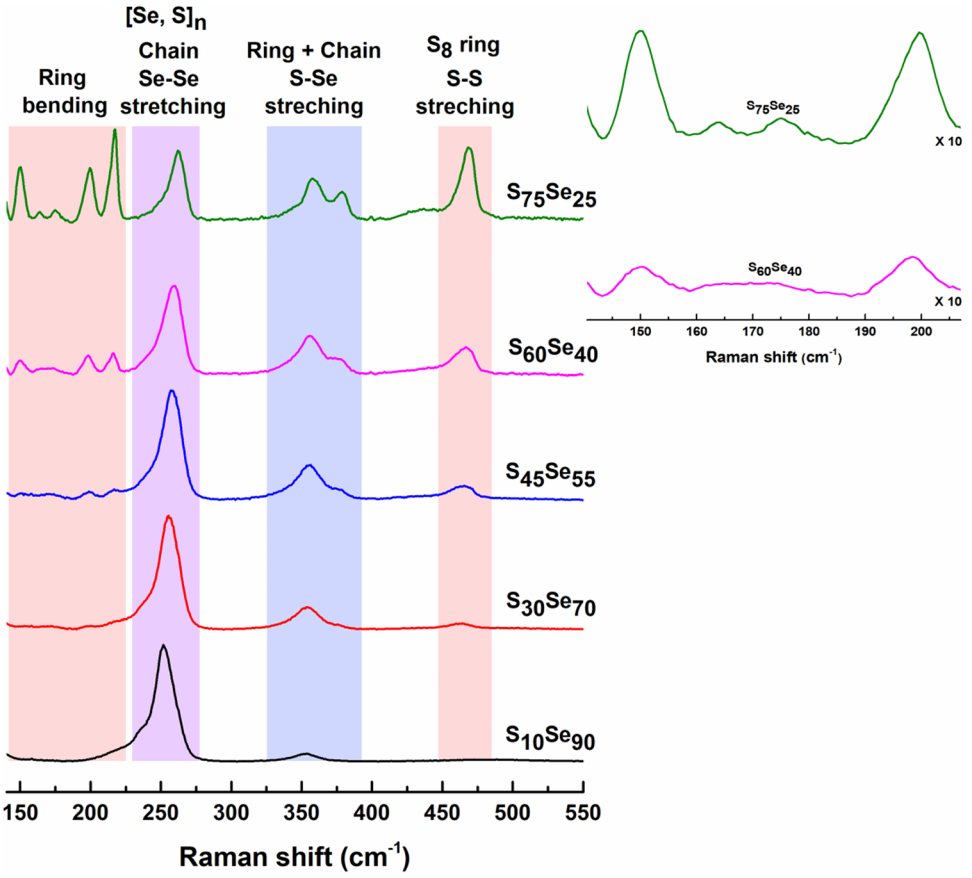

Figure 6. Unpolarized Raman spectra of S_xSe_{100-x} glasses. Inset to the right shows a magnified (10×) view of the ring bending modes in $S_{60}Se_{40}$ (bottom) and $S_{75}Se_{25}$ (top) glasses.

suggested that the concentration of the Se_2S_6 rings increases with increasing Se concentration, with the relative abundances of the Se_1S_7 and the Se_2S_6 rings becoming comparable at ∼40 at. % Se.[20] On the other hand, the Se ring speciation in S_xSe_{100-x} glasses, as obtained in this study, shows that the average ring composition is Se_1S_7 at low S (high Se) concentration and it becomes $Se_{1.5}S_{6.5}$, thus suggesting an increased fraction of Se_2S_6 rings and possibly rings with even higher Se content (e.g., Se_3S_5 and Se_4S_4) in glasses with ≤40 at. % Se. As discussed below, the Raman spectroscopic results are consistent with this structural model.

3.3. Raman Spectroscopy. The Raman spectra of the binary S_xSe_{100-x} glasses are shown in Figure 6. All spectra contain a relatively strong band centered near ∼250 to 260 cm^{-1} that can be readily assigned to the symmetric Se−Se bond-stretching mode in $[Se]_n$ chains.[40] The incorporation of S in these $[Se]_n$ chains is presumably reflected in the progressive shift of the frequency of this band from 251 to 261 cm^{-1} with increasing S concentration (Figure 6). This result is also corroborated by the fact that the ^{77}Se NMR spectra of all glasses contain the resonance corresponding to the $[Se,S]_n$ chains (Figure 2b). The relatively narrow and strong vibrational bands located at ∼150 and 216 cm^{-1} in the Raman spectra of the high sulfur containing glasses are characteristic of S_8 rings typical of crystalline S and correspond to the antisymmetric and symmetric bending modes (Figure 6).[8,21] These vibrational bands are accompanied by another strong and narrow band near 202 cm^{-1} in the glass spectra in Figure 6. Additionally, two more bands in the spectral region between 160 and 190 cm^{-1} appear in the Raman spectrum of the $S_{60}Se_{40}$ glass and become clearly resolved near 163 and 175 cm^{-1} in the spectrum of the $S_{75}Se_{25}$ glass (see Figure 6, inset). The frequencies of these three bands at 202, 175, and 163 cm^{-1} agree well with those predicted respectively for the bending of Se_1S_7, Se_2S_6, and Se_3S_5 rings by Ward in a previous Raman spectroscopic study of S_xSe_{100-x} crystals and melts.[17] These predictions are based on the model proposed by Ward, which assumed a linear scaling of the ring bending frequency with the average force constant and with the inverse square root of the molecular weight of the ring, where the average force constant was further assumed to vary linearly with the degree of substitution of S with Se in the Se_yS_{8-y} ring.[17] This structural assignment of these vibrational bands and their relative intensities in Figure 6 clearly suggest the predominance of the Se_1S_7 rings among the Se-substituted Se_yS_{8-y} ring environments in S_xSe_{100-x} glasses. Moreover, the appearance of Se_2S_6 and Se_3S_5 rings in glasses with the highest S contents suggests increasing incorporation of multiple Se atoms in the Se_yS_{8-y} rings. These results are qualitatively completely consistent with the scenario of the evolution of the average Se_yS_{8-y} ring composition in S_xSe_{100-x} glasses, as obtained from the ^{77}Se NMR results discussed above.

It is apparent from the Raman spectra in Figure 6 that increasing S content also results in a concomitant increase in the intensity of the band near 468 cm^{-1}, corresponding to the symmetric S−S bond-stretching mode for the S_8 rings.[8] In addition, two more bands centered at ∼360 and 379 cm^{-1} with a weak band present as a shoulder near 340 cm^{-1} display a

DOI: 10.1021/acs.jpcb.8b10052
J. Phys. Chem. B 2018, 122, 12219−12226

similar behavior of increasing intensity with S content (Figure 6). Previous Raman spectroscopic studies of S_xSe_{100-x} crystals have assigned these bands to S−Se stretches as these frequencies are intermediate between the S−S stretching near 470 cm^{-1} and Se−Se stretches near 260 cm^{-1}.[17,18] As such, the presence of these bands directly implies mixing between S and Se in the chain and ring elements in the structure.

In general, the Raman bands in the 340−380 cm^{-1} region in these materials are believed to represent two types of S−Se stretching modes: (i) strongly coupled S−Se stretches in −S−Se−S− linkages are manifested as vibrational bands near ∼340 and 380 cm^{-1} while (ii) isolated S−Se stretches in −S−Se−Se−S− moieties appear as a band near ∼360 cm^{-1}.[18,41,42] It is noteworthy that previous studies of binary S−Se crystals concluded that both coupled and isolated S−Se stretching bands are from Se_yS_{8-y} ring molecules with adjacent Se atoms in −S−Se−Se−S− moieties being the preferred bonding scenario if more than one Se atom is present in these rings.[19,21] As shown in Figure 6, the intensity of the vibrational bands in the 340−380 cm^{-1} region is increasing significantly with increasing sulfur content. This observation indicates that a significant fraction of Se atoms is incorporated into the Se_yS_{8-y} ring structures as −S−Se−S− and −S−Se−Se−S− linkages, when sufficient sulfur is present in the system. Moreover, both Se_1S_7 and Se_2S_6 type rings may coexist in the structure. These conclusions are completely consistent with the structural model proposed above on the basis of the ^{77}Se NMR spectroscopic results. Finally, it may be noted that the band near 360 cm^{-1}, corresponding to S−Se stretches in −S−Se−Se−S− moieties, has a noticeable presence even in the Raman spectra of glasses with low sulfur concentration (S ≤ 30 at. %) that have rather weak or no signature of the vibrational bands corresponding to the Se_yS_{8-y} rings (Figure 6). This result suggests that all of the −S−Se−Se−S− moieties corresponding to the 360 cm^{-1} band may not belong to the Se_yS_{8-y} ring elements in the structure, but a significant fraction likely belong to the $[Se,S]_n$ chain elements.

4. CONCLUSIONS

The structure of S_xSe_{100-x} glasses consists of copolymeric $[S,Se]_n$ chains and heterocyclic S_ySe_{8-y} rings. Se and S atoms show strong preference to form the chain and the ring elements, respectively, which prevents a random or homogeneous mixing between these two elements. The compositional variation of the chain versus ring speciation of Se atoms is consistent with an average ring composition of Se_1S_7 in glasses with ≤40 at. % S. Further increase in S content results in the incorporation of more Se atoms in the ring elements, resulting in an average ring composition of $Se_{1.5}S_{6.5}$. It is, however, not the peculiar chemical order between S and Se but the total chain versus ring content in the structure that controls both the packing and the mobility of the constituent structural units. As the total chain content increases with increasing Se concentration in these glasses, the stronger interaction between the chain elements compared to rings results in less efficient atomic packing and lower mobility, which are manifested in the decreasing molar volume and increasing T_g, respectively.

AUTHOR INFORMATION

Corresponding Author

*(S.S.) E-mail: sbsen@ucdavis.edu.

ORCID

Sabyasachi Sen: 0000-0002-4504-3632

Notes

The authors declare no competing financial interest.

ACKNOWLEDGMENTS

This work was supported by the National Science Foundation Grant NSF-DMR 1505185. The National High Magnetic Field Laboratory is supported by National Science Foundation through NSF DMR-1644779 and the State of Florida.

REFERENCES

(1) Zakery, A.; Elliott, S. R. Optical Properties and Applications of Chalcogenide Glasses: A Review. *J. Non-Cryst. Solids* **2003**, *330*, 1−12.

(2) Bureau, B.; Zhang, X. H.; Smektala, F.; Adam, J. L.; Troles, J.; Ma, H. L.; Boussard-Plèdel, C.; Lucas, J.; Lucas, P.; Le Coq, D.; et al. Recent Advances in Chalcogenide Glasses. *J. Non-Cryst. Solids* **2004**, *345−346*, 276−283.

(3) Calvez, L. Chalcogenide Glasses and Glass-Ceramics: Transparent Materials in the Infrared for Dual Applications. *C. R. Phys.* **2017**, *18*, 314−322.

(4) Popescu, M. *Non-Crystalline Chalcogenides*; Kluwer Academic Publishers: New York, 2002.

(5) Greer, S. C. Reversible Polymerizations and Aggregations. *Annu. Rev. Phys. Chem.* **2002**, *53*, 173−200.

(6) Greer, S. C. Living" Polymers. *Adv. Chem. Phys.* **2007**, *94*, 261.

(7) Sofekun, G. O.; Evoy, E.; Lesage, K. L.; Chou, N.; Marriott, R. A. The Rheology of Liquid Elemental Sulfur Across the λ-Transition. *J. Rheol.* **2018**, *62*, 469−476.

(8) Kalampounias, A. G.; Andrikopoulos, K. S.; Yannopoulos, S. N. Probing the Sulfur Polymerization Transition In Situ with Raman Spectroscopy. *J. Chem. Phys.* **2003**, *118*, 8460−8467.

(9) Lucovsky, G.; Mooradian, A.; Taylor, W.; Wright, G. B.; Keezer, R. C. Identification of the Fundamental Vibrational Modes of Trigonal, α-Monoclinic and Amorphous Selenium. *Solid State Commun.* **1967**, *5*, 113−117.

(10) Marple, M.; Badger, J.; Hung, I.; Gan, Z.; Kovnir, K.; Sen, S. Structure of Amorphous Selenium by 2D ^{77}Se NMR Spectroscopy: An End to the Dilemma of Chain versus Ring. *Angew. Chem.* **2017**, *129*, 9909−9913.

(11) Bureau, B.; Danto, S.; Ma, H. L.; Boussard-Plédel, C.; Zhang, X. H.; Lucas, J. Tellurium Based Glasses: A Ruthless Glass to Crystal Competition. *Solid State Sci.* **2008**, *10*, 427−433.

(12) Brodsky, M. H.; Gambino, R. J.; Smith, J. E.; Yacoby, Y. The Raman Spectrum of Amorphous Tellurium. *Phys. Status Solidi B* **1972**, *52*, 609−614.

(13) Grison, E. Studies on Tellurium-Selenium Alloys. *J. Chem. Phys.* **1951**, *19*, 1109−1113.

(14) Bureau, B.; Boussard-Plèdel, C.; Lefloch, M.; Troles, J.; Smektala, F.; Lucas, J. Selenium-Tellurium Sequences in Binary Glasses as Depicted by ^{77}Se and ^{125}Te NMR. *J. Phys. Chem. B* **2005**, *109*, 6130−6135.

(15) Tverjanovich, A.; Cuisset, A.; Fontanari, D.; Bychkov, E. Structure of Se-Te Glasses by Raman Spectroscopy and DFT Modeling. *J. Am. Ceram. Soc.* **2018**, *101*, 5188−5197.

(16) Jecu, D.; Jaklovszky, J.; Trutia, A.; Apostol, I.; Dinescu, M.; Mihailescu, I. N.; Aldica, G.; Popescu, M.; Vlahovici, N.; Zamfira, S.; Indrea, E. Preparation, Structure and Optical Properties of Glasses in the Systems Selenium-Sulfur and Tellurium-Sulfur. *J. Non-Cryst. Solids* **1987**, *90*, 319−322.

(17) Ward, A. T. Raman Spectroscopy of Sulfur, Sulfur-Selenium, and Sulfur-Arsenic Mixtures. *J. Phys. Chem.* **1968**, *72*, 4133−4139.

(18) Laitinen, R.; Steudel, R. Vibrational Spectroscopic Investigations of S_nSe_{n-8} Molecules. *J. Mol. Struct.* **1980**, *68*, 19−32.

DOI: 10.1021/acs.jpcb.8b10052
J. Phys. Chem. B 2018, 122, 12219−12226

(19) Laitinen, R. S.; Pakkanen, T. A. ^{77}Se NMR Spectroscopic Characterization of Selenium Sulfide Ring Molecules Se_nS_{8-N}. *Inorg. Chem.* **1987**, *26*, 2598−2603.
(20) Chivers, T.; Laitinen, R.; Schmidt, K. Se NMR Spectroscopic Study of the Molecular Composition of Sulfur-Selenium Melts. *Can. J. Chem.* **1992**, *70*, 719−725.
(21) Steudel, R.; Laitinen, R. Cyclic Selenium Sulfides. In *Inorganic Ring Systems*; Chivers, T., Keat, R., Labarre, J.-F., Laitinen, R., Lavrent'yev, V. I., Oakley, R. T., Steudel, R., Voronkov, M. G., Eds.; Springer: Berlin, 1982; pp 177−197.
(22) Hung, I.; Edwards, T.; Sen, S.; Gan, Z. MATPASS/CPMG: A Sensitivity Enhanced Magic-Angle Spinning Sideband Separation Experiment for Disordered Solids. *J. Magn. Reson.* **2012**, *221*, 103−109.
(23) States, D. J.; Haberkorn, R. A.; Ruben, D. J. A 2D Nuclear Overhauser Experiment with Pure Absorption Phase in Four Quadrants. *J. Magn. Reson.* **1982**, *48*, 286−292.
(24) Harris, R. K.; Becker, E. D.; De Menezes, S. M. C.; Goodfellow, R.; Granger, P. NMR Nomenclature. Nuclear Spin Properties and Conventions for Chemical Shifts - (IUPAC Recommendations 2001). *Pure Appl. Chem.* **2001**, *73*, 1795−1818.
(25) Haeberlen, U. *High Resolution NMR in Solids Selective Averaging: Supplement 1 Advances in Magnetic Resonance*; Elsevier: Burlington, MA, 2012.
(26) Buler, P. I.; Kuleshov, E. A.; Protasova, L. G. Molar Volume of Glasses in the Se-S System. *Fiz. i Khimiya Stekla* **1984**, *10*, 628−630.
(27) Protasova, L. G.; Kuleshov, E. A.; Buler, P. I.; Vlasova, S. G. Thermal Expansion and the Glass-Formation Temperature of Glasses in the Se-S System. *Fiz. i Khimiya Stekla* **1986**, *12*, 168−171.
(28) Buler, P. I.; Protasova, L. G.; Shaposhnikova, I. G. Thermal Capacity of Glasses of the System Se-S in the Temperature Interval 173−333K. *Fiz. i Khimiya Stekla* **1986**, *12*, 544−548.
(29) Svoboda, R.; Málek, J. Kinetic Fragility of Se-Based Binary Chalcogenide Glasses. *J. Non-Cryst. Solids* **2015**, *419*, 39−44.
(30) Abrahams, S. C. The Crystal and Molecular Structure of Orthorhombic Sulfur. *Acta Crystallogr.* **1955**, *8*, 661−671.
(31) Vedam, K.; Miller, D. L.; Roy, R. Elastic Constants of Selenium in the Hexagonal and Glassy Phases. *J. Appl. Phys.* **1966**, *37*, 3432−3434.
(32) Zhu, W.; Lockhart, M.; Aitken, B.; Sen, S. Dynamical Rigidity Transition in the Viscoelastic Properties of Chalcogenide Glass-Forming Liquids. *J. Non-Cryst. Solids* **2018**, *502*, 244−248.
(33) Bureau, B.; Troles, J.; Le Floch, M.; Smektala, F.; Lucas, J. Medium Range Order Studied in Selenide Glasses by 77Se NMR. *J. Non-Cryst. Solids* **2003**, *326-327*, 58−63.
(34) Massiot, D.; Fayon, F.; Capron, M.; King, I.; Le Calvé, S.; Alonso, B.; Durand, J. O.; Bujoli, B.; Gan, Z.; Hoatson, G. Modelling One- and Two-Dimensional Solid-State NMR Spectra. *Magn. Reson. Chem.* **2002**, *40*, 70−76.
(35) Kaseman, D. C.; Hung, I.; Gan, Z.; Sen, S. Observation of a Continuous Random Network Structure in Ge_xSe_{100-x} Glasses: Results from High-Resolution ^{77}Se MATPASS/CPMG NMR Spectroscopy. *J. Phys. Chem. B* **2013**, *117*, 949−954.
(36) Bonhomme, C.; Gervais, C.; Babonneau, F.; Coelho, C.; Pourpoint, F.; Azaïs, T.; Ashbrook, S. E.; Griffin, J. M.; Yates, J. R.; Mauri, F.; et al. First-Principles Calculation of NMR Parameters Using the Gauge Including Projector Augmented Wave Method: A Chemists Point of View. *Chem. Rev.* **2012**, *112*, 5733−5779.
(37) Warren, B. E.; Burwell, J. T. The Structure of Rhombic Sulphur. *J. Chem. Phys.* **1935**, *3*, 6−8.
(38) Clark, S. J.; Segall, M. D.; Pickard, C. J.; Hasnip, P. J.; Probert, M. I. J.; Refson, K.; Payne, M. C. First Principles Methods Using CASTEP. *Z. Kristallogr. - Cryst. Mater.* **2005**, *220*, 567−570.
(39) Perdew, J. P.; Burke, K.; Ernzerhof, M. Generalized Gradient Approximation Made Simple. *Phys. Rev. Lett.* **1996**, *77*, 3865−3868.
(40) Yannopoulos, S. N.; Andrikopoulos, K. S. Raman Scattering Study on Structural and Dynamical Features of Noncrystalline Selenium. *J. Chem. Phys.* **2004**, *121*, 4747−4758.
(41) Laitinen, R.; Niinistö, L.; Steudel, R. Structural Studies on the Sulfur-Selenium Binary Systerm. *Acta Chem. Scand.* **1979**, *33*, 737−747.
(42) Laitinen, R.; Pakkanen, T. A. Theoretical Investigation of the Sulfur-Selenium Bond. *J. Mol. Struct.: THEOCHEM* **1983**, *91*, 337−352.

DOI: 10.1021/acs.jpcb.8b10052
J. Phys. Chem. B 2018, 122, 12219−12226